Coastal Engineering 213 (2027) 105170

Contents lists available at ScienceDirect

Coastal Engineering

journal homepage: www.elsevier.com/locate/coastaleng

Physical experiments on dune erosion under rising storm surge levels

Björn Mehrtens [a,*], Oliver Lojek [a], Lukas Ahrenbeck [a], Viktoria Kosmalla [a], Thea Bölker [a], David Schürenkamp [a], Nils Goseberg [a,b]

[a] Technische Universität Braunschweig, Leichtweiß-Institute for Hydraulic Engineering and Water Resources; Division of Hydromechanics, Coastal and Ocean Engineering, Beethovenstraße 51a, Braunschweig, 38106, Germany

[b] Coastal Research Center, Joint Central Institution of Leibniz Universität Hannover and Technische Universität Braunschweig, Merkurstraße 11, Hannover, 30419, Germany

ARTICLE INFO

Keywords:
Coastal dunes
Sea level rise
Physical experiments
Dune erosion

ABSTRACT

Coastal dunes are key components of nature-based coastal protection, but they face increasing risk from sea-level rise driven by climate change. This study investigates the morphodynamic response of a bare coastal dune model to five storm surge cases with progressively rising still water levels (SWLs) reflecting local sea level rise (SLR) projections in 1:7 scaled physical experiment series. Results reveal a systematic transition in flooding and erosion hazard regimes from localized, collision-induced dune retreat under current standard storm surge levels to major overwash and partial dune breaching under SLR projections of up to +1.2 m by 2100. Characteristic dune erosion processes of periodic scarping, notching, and slumping were found to migrate vertically with rising SWLs, progressively relocating the dune crest and increasing risk of breaching. Beyond quantifying total dune erosion volumes, this study introduces the proportion of eroded dune area above the still water level as a complementary indicator of residual dune protective capacity. Compared with the conventional erosion volume, this indicator more directly reflects the remaining protective dune volume available to resist overtopping and breaching during extreme events. Overall, the findings highlight the increasing vulnerability of natural dunes in the context of climate change-driven sea-level rise and underscore the urgent need for improved risk assessments and adaptive management strategies to preserve sufficient dune resilience and maintain their coastal protection function.

1. Introduction

Coastal dunes are widespread, global landforms along sandy coasts evolving across a wide range of spatio-temporal scales, driven by complex biophysical interaction between sediment supply, wind, and vegetation (Hesp, 2002; Zarnetske et al., 2015). In addition to providing various ecosystem services such as biodiversity support (Gracia et al., 2018), habitat and freshwater provision (Barbier et al., 2011; Nehren et al., 2016), coastal dunes act as protective buffers for many low-lying coastal communities during storm surge events (De Jong et al., 2014; Figlus et al., 2022). As defined by the International Union for Conservation of Nature (IUCN), dunes are categorized as a soft "nature-based solution" (NBS) for coastal protection that in contrast to hard engineering structures consist of partially vegetation covered unconsolidated sand and reduce coastal risks and prevent flooding (Huynh et al., 2024; Sedrati et al., 2025). Against the background of global climate change, associated rising sea levels (Calafat et al., 2022) and intensifying storm frequencies (Vousdoukas et al., 2020) as well as exacerbated coastal squeeze (Lansu et al., 2024), the protective value of such natural and adaptive defense measures has increasingly been recognized by policy makers in recent past (Hanley et al., 2014). To ensure a sufficient dune safety level under these projections in the future, a comprehensive understanding of dune erosion processes is crucial for reliable coastal hazard mitigation (Maximiliano-Cordova et al., 2023; Conti et al., 2024). However, despite recent advances in process-based numerical modeling (Liang et al., 2023; Irish et al., 2024; Ma et al., 2024), new insights into specific dune erosion processes remain essential to conceptualize and validate the role of coastal dunes as protective barriers (Toledo et al., 2024).

To classify the morphological response of beach–dune systems subjected to varying storm conditions, Sallenger (2000) defined four regimes of wave-dune interaction based on the relation between the

* Corresponding author.
E-mail addresses: b.mehrtens@tu-braunschweig.de (B. Mehrtens), o.lojek@tu-braunschweig.de (O. Lojek), lukas.ahrenbeck@tu-braunschweig.de (L. Ahrenbeck), v.kosmalla@tu-braunschweig.de (V. Kosmalla), thea.boelker@tu-braunschweig.de (T. Bölker), d.schuerenkamp@tu-braunschweig.de (D. Schürenkamp), n.goseberg@tu-braunschweig.de (N. Goseberg).

https://doi.org/10.1016/j.coastaleng.2026.105170
Received 6 March 2026; Received in revised form 2 October 2026; Accepted 6 October 2026
Available online 16 October 2026
0378-3839/© 2026 The Authors. Published by Elsevier B.V. This is an open access article under the CC BY license (http://creativecommons.org/licenses/by/4.0/).
Open access funding enabled and organized by Projekt DEAL.

dune crest height and the extent of wave run-up. The four regimes include: (1) *swash*, where run-up and erosion is confined to the foreshore; (2) *collision*, where run-up collides with the dune face forcing erosion and seaward directed sediment transport; (3) *overwash*, where run-up overtops the dune causing water flow induced erosion and landward sediment deposition; (4) *inundation*, where the dune is completely submerged. More recently, Leaman et al. (2021) expanded this existing approach with four flooding hazard regimes by proposing four new erosion hazard regimes to explicitly include the contribution of wave-induced morphological changes to a total storm hazard. The definition of the erosion hazard scale is based on the horizontal recession of sandy beaches and dunes during a storm and categorized into the following regimes: (1) *minor beach narrowing*, where a reduction in beach width does not affect the dune system; (2) *substantial beach narrowing*, where the dune system remains intact but potentially vulnerable to subsequent storms; (3) *dune face erosion*, where erosion occurs landward from the dune toe without impacting the dune crest; (4) *dune retreat*, where severe erosion impacts the landward side of the dune crest.

Besides field measurements (Maximiliano-Cordova et al., 2021; Harley et al., 2022; Van Wiechen et al., 2024), physical model experiments under controllable boundary conditions are fundamental methods for data acquisition of complex wave-dune interaction phenomena (D'Alessandro et al., 2022; Maximiliano-Cordova et al., 2023). Previous laboratory studies on dune erosion were performed over a wide range of model scales, addressing aspects such as varying beach-dune geometries (Figlus et al., 2011; Dionísio António et al., 2023), hydrodynamic forces (Van Gent et al., 2008; D'Alessandro and Tomasicchio, 2016), vegetation effects (Bryant et al., 2019; Figlus et al., 2022; Feagin et al., 2023), and hybrid dune core reinforcements (Odériz et al., 2020; Maximiliano-Cordova et al., 2023; Ghasemi et al., 2024). The majority of experimental studies focused on collision (Figlus et al., 2022; Bond et al., 2023; Lee et al., 2024; Conti et al., 2024) and overwash (Figlus et al., 2011; Liang et al., 2023) regimes, as these are crucial in determining the protective capacity of dunes under storm impacts (Leaman et al., 2021). Dune erosion mechanisms under prevailing collision regime have been studied extensively in various laboratory experiments with unvegetated dune models (Erikson et al., 2007; D'Alessandro and Tomasicchio, 2016; Bond et al., 2023; Conti et al., 2024; Lee et al., 2024), observing characteristic phases of wave-induced scarp migration, notching, and dune face collapsing (also called slumping). After incident wave run-up erodes the dune face and forms a vertical scarp, ongoing wave attack causes an undercutting at the toe (notching), leaving an unstable mass of sediment above the notch. Subsequent dune face collapsing (slumping) occurs when a portion of the overhang collapses downward into the swash zone, providing temporary protection until further wave action gradually erodes the sediment and ultimately deposits it off- or longshore (Van Wiechen et al., 2024). The process of scarping, notching, slumping and sediment removal appears episodically with individual slumps, until the prevailing wave energy diminishes, halting further dune erosion. In this regard, Conti et al. (2024) emphasized that higher water levels increase the number of slumps and have a more pronounced impact on erosion magnitude compared to wave conditions (Van Gent et al., 2008; D'Alessandro and Tomasicchio, 2016) and moisture content. As part of physical experiments using an overwash regime with elevated water levels and wave conditions, D'Alessandro and Tomasicchio (2016) observed severe wave overtopping, causing rapid dune erosion, crest lowering, and dune breaching, ultimately exposing the landward side to larger waves and flooding (Berard et al., 2017). Furthermore, Liang et al. (2023) demonstrated a linear relation between the overwash water volume and the deposited sediment volume as well as a proportional relation between the erosion volume and the wave energy flux. While some experimental model setups deliberately omitted prototype scaling of beach-dune geometries, water levels, and wave characteristics to enable targeted investigations of specific storm regimes (D'Alessandro and Tomasicchio, 2016; Berard et al., 2017), moisture contents (Conti et al., 2024) or vegetation metrics (Bryant et al., 2019; Figlus et al., 2022) employing controllable conditions, various studies focused on replicating coastal erosion of idealized beach-dune systems under representative storm events. A prevalent methodology involves scaling registered storm wave and water-level hydrographs using Froude similitude, and imposing the scaled conditions onto a simplified scaled beach-dune profile derived from field surveys to reproduce morphodynamic responses encountered (Palmsten and Holman, 2012; Silva et al., 2016; Bond et al., 2023; Feagin et al., 2023; Lee et al., 2024). In this regard, the covariation of water levels and wave conditions complicates the ability to isolate and quantify the individual contributions of each variable to dune erosion dynamics (Conti et al., 2024).

Building upon these previous studies, the objective of this study is to improve the process-based understanding of dune erosion under progressively increasing still water levels representative of projected sea-level rise scenarios. Rather than evaluating the overall capacity of coastal dunes to provide flood protection under future climate change, the experiments aim to investigate how increasing still water levels influence characteristic erosion mechanisms, hazard regime transitions and residual dune protective capacity under representative storm conditions. To address this overarching goal, this study presents a novel 1:7 scaled physical experiment series with a geometrically-representative beach-dune profile from the German North Sea Coast (Mehrtens et al., 2023) subjected to representative storm surge conditions, while explicitly incorporating projected SLR scenarios through the year 2100. In addition, the experiments consider two consecutive storm events with increasing wave conditions to represent a conservative storm clustering within a single storm season (Dissanayake et al., 2015). The experimental design intentionally assumes that the second storm occurs before any significant post-storm morphological recovery of the dune or human intervention could have occurred. Consequently, the second event acts on an already eroded dune with reduced protective capacity, allowing the cumulative effects of repeated storm events on the residual flood protection to be investigated independently of recovery processes, which were beyond the scope of the present study. The study pursues four specific objectives:

(i.) to quantify erosion progression during two successive storms events of intensifying wave conditions,
(ii.) to investigate changes in dune erosion dynamics under rising water levels associated with SLR,
(iii.) to examine the influence of elevated water levels on flooding and erosion hazard scales, and
(iv.) to assess the resulting implications of these changes for dune vulnerability and their effectiveness as natural flood protection features under future climate conditions.

2. Materials and methods

2.1. Modeling of beach-dune profile

A geometrically-representative beach-dune profile was derived from an established natural coastal dune system at the west coast of the Eiderstedt peninsula, Germany (Mehrtens et al., 2023). This region is located at the North Frisian Wadden Sea, featuring a meso-tidal environment with an average tidal range of 3.0 m near the coast (Jänicke et al., 2021). Local bathymetry data was obtained from the EasyGSH-DB portal for the year 2016 with a resolution of 10 × 10 m (Sievers et al., 2020). As shown in Fig. 1.1, the study area encompasses a coastal landscape, featuring a 400–2,000 m^2 wide sandy beach, a foredune system lining the beach along 6.5 km colonized by marram grass communities, followed by a low-lying salt marsh lagoon spanning 17,500 m^2 with several tidal channels, concluded on the landward side by an established dune system with a dense vegetation cover including a coniferous dune forest. The flat beach, with an average elevation

height of 1.9 m above the German reference level NHN (standard elevation zero) spans 12 km in length and up to 2 km in width, exposing a large area to aeolian sediment transport. As reported by Mehrtens et al. (2023), these morphodynamic conditions promoted the spatial development of the foredune chain over recent decades. The foredune exhibits varying dune heights, with crest elevations reaching up to 11 m +NHN and blowouts near the beach level creating natural pathways for potential flooding of the hinterland during storm surge events. The established dune system landward to the salt marsh extends parallel to the shoreline for 1.3 km (Mehrtens et al., 2023), bridging the local dike lines in the north and the south; this dune system provides exclusive storm surge protection along this stretch. In order to perform 2D experimental tests in a wave flume, a representative cross-shore beach-dune transect has been extracted from the local bathymetry covering the beach, the foredune, the salt marsh as well as the established dune (see Fig. 1.2). The illustrated transect was chosen at the lowest crest elevation of the established dune, where the foredune is relatively low with a nearby blowout, and without a well-developed dune forest at the dike transition. Therefore, the transect characterizes a more vulnerable section along the dune stretch, where severe storm events can potentially cause extensive dune erosion leading to dune breaching and flooding of the hinterland. As additionally shown in Fig. 1.2, a defined severe storm surge ranges from 2.5 m to 3.5 m above the local mean high water of approximately 1.6 m +NHN (Mehrtens et al., 2023). For the performance of experimental studies, a prototype dune profile was derived by focusing on the seaward most ridge of the established dune, as it has the highest elevation and serves as the primary line of defense against incoming waves. All other landscape features, including the beach, the foredune, the salt marsh, and the dune forest were excluded from the modeling process. Consistent with several previous studies (D'Alessandro et al., 2022; Bond et al., 2023), no vegetation cover was considered, resulting in a bare sand dune measuring 5.6 m in height and 85.4 m in length, with a local sediment grain size of 0.245 mm (see Fig. 1.3).

2.2. Modeling of hydrodynamic conditions

Prototype hydrodynamical boundary parameters from the study area were determined for representative scaling of characteristic storm surge forces. As listed in Fig. 2.1, design storm surge levels defined by local coastal authorities with return periods of 50 to 200 years range between 4.85 m +NHN and 5.20 m +NHN. Four different local sea level rise projections for the years 2050 and 2100 were considered, referring to RCP4.5 and RCP8.2 scenarios (Gaslikova et al., 2013). By combining these parameters, an overview matrix with a total of 15 potential storm surge levels (SSLs) has been created ranging from 4.85 m +NHN to 6.40 m +NHN. For comparison, the highest storm surge level in recent past has been recorded in 1976 with a maximum SSL of 4.80 m +NHN. Based on the designed matrix, 5 storm cases A–E were selected for experimental model tests to cover a wide range of scenarios. In order to investigate the influence of two consecutive storm surges with intensifying wave conditions, two representative significant wave heights H_s and peak periods T_p for the study area were adopted from Hagen et al. (2020). These wave conditions represent typical mean local wave characteristics and were selected to provide representative hydrodynamic forcing for the investigated storm surge scenarios. The wave conditions were defined as follows: test series 1 with $H_{s,1}$ = 0.80 m and $T_{p,1}$ = 6.0 s; test series 2 with $H_{s,2}$ = 1.10 m and $T_{p,2}$ = 7.0 s (see Fig. 2.2). Fig. 2.3 shows a prototype time series from a storm surge event in 2013 recorded at nearby gauging station with an maximum SSL of 4.45 m +NHN. Based on this recording and in accordance with normative storm surge events at the Dutch coast (Van Gent et al., 2008) a single prototype storm surge duration of 5 h has been defined for both consecutive test series.

Table 1
Scaling of boundary conditions for the beach-dune profile and hydrodynamics.

			Prototype	Model	Scale factor
Beach-dune profile					
Beach elevation	h_{beach}	(m + NHN)	1.9	0.27	7
Dune volume	V_{dune}	(m^3)	1334	3.89	7^3
Dune height	h_{dune}	(m)	5.6	0.8	7
Grain size	d_{50}	(mm)	0.25	0.12	2.04
Hydrodynamics					
Storm surge duration	t_{SSL}	(min)	300	113	$\sqrt{7}$
Storm surge level SSL	h_{SSL}	(m + NHN)	4.85–6.05	0.69–0.86	7
Still water depth	d	(m)	2.95–4.15	0.42–0.59	7
Sig. wave height	H_s	(m)	0.75–1.10	0.105–0.155	7
Peak period	T_p	(s)	6.3–7.0	2.4–2.65	$\sqrt{7}$

2.3. Experimental setup and program

Physical model tests were conducted in a wave flume at the Leichtweiß-Institute for Hydraulic Engineering and Water Resources, Technische Universität Braunschweig, Germany. The flume is 2 m wide, 1.5 m high, 90 m long and features a piston-type wave maker (VTI, Spain, with Aalborg wave generation software Awasys v.7) to generate irregular JONSWAP spectra (γ = 3.3). The designed dune model with a length of x = 12.2 m, a width of y = 2.0 m and crest height of z = 0.8 m was constructed near the end of the flume (distance of 71 m from the wave maker to the dune toe) with the simplification of the mean beach elevation corresponding to the plane height of the flume bottom (see Fig. 1.4 and .5). Apart from the sediment grain size, the dune profile scaling followed Froude's similarity law with a length scale factor of λ_l = 7 (see Table 1). A fine, non-cohesive well sorted sand (uniformity coefficient C_u = 1.59) with a medium grain size d_{50} of 0.12 mm (d_{10} = 0.087 mm, d_{90} = 0.183 mm) and a calculated settling velocity w_f of 8.4 mm/s was used for the dune model. The sand was selected according to established movable-bed modeling practice with a minimum Dean coefficient of $A > 5$ for dissipative profiles and the requirement to simulate transitional flow conditions ($0.5 < Re < 400$) (Soulsby, 1997), rather than applying strict geometric scaling of the prototype grain size. This approach enables representative wave-induced sediment transport and beach-dune morphodynamics under Froude-scaled conditions, although complete similitude of prototype sediment mobility and transport rates cannot be achieved. Prior to each experiment, the dune model was manually reconstructed to its initial geometry using the predefined profile template. No dedicated assessment of sediment compaction or bulk density was performed. Corresponding to the beach-dune profile scaling, hydrodynamic conditions were also selected by applying Froude similitude with an identical length scale factor of λ_l = 7 (see Table 1). By subtracting the mean beach elevation from the defined prototype storm surge levels (SSLs) of storm cases A–E (see Fig. 2.1), the corresponding still water levels (SWLs) applied in the physical experiments ranged from d = 0.42 m to d = 0.59 m.

A single test for each storm case was split in two sequential wave time histories (test series 1 with $H_{s,1}$ = 10.5 cm and $T_{p,1}$ = 2.4 s; test series 2 with $H_{s,2}$ = 15.5 cm and $T_{p,2}$ = 2.65 s), each running for 113 min to simulate two consecutive storm surge events with intensifying wave conditions. Except for the storm case E with the highest water depth of d = 0.59 m, the test runs for all storm cases A–D were performed twice to ensure reproducibility (see Table 2).

2.4. Instrumentation

The wave flume was equipped with five wave gauges along the flume center line to measure incident wave conditions at a sampling frequency of 60 Hz. Two side-viewing cameras (HiLook IPC-B650H-Z with 5-megapixel resolution of 2560 × 1920) were placed outside the

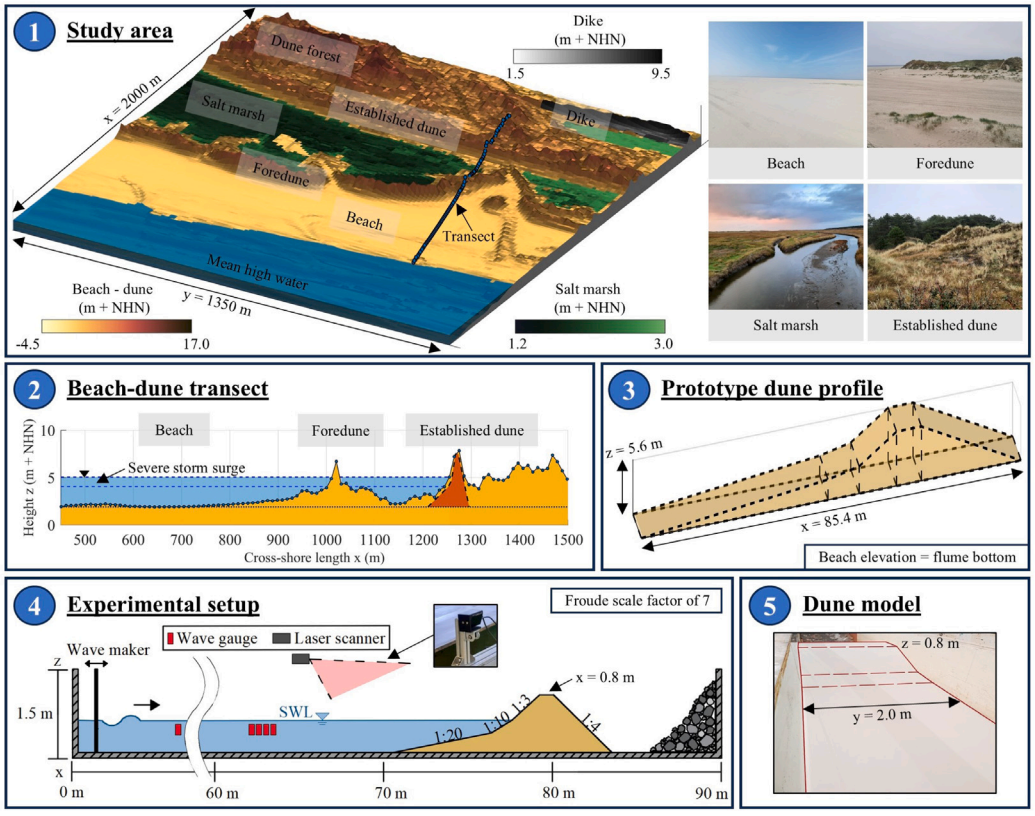


Fig. 1. Design of a representative dune model including: (1) the focused study area at the Eiderstedt peninsula; (2) a cross-shore view of the extracted beach-dune transect from the field; (3) the defined prototype dune profile for the established dune; (4) a cross-shore view of the experimental setup along the wave flume and (5) a photograph of the constructed dune model.

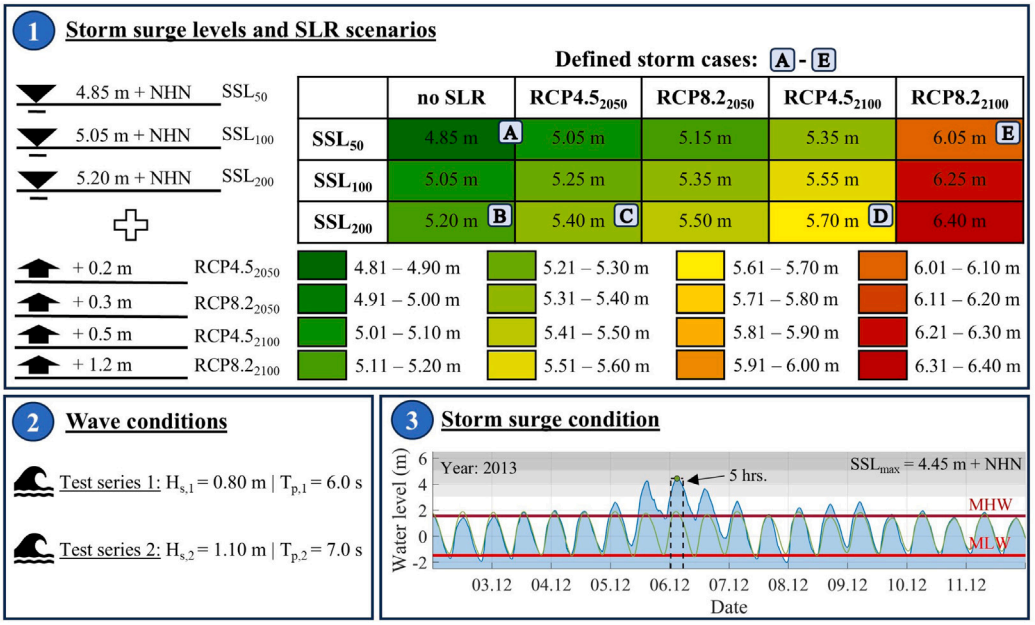


Fig. 2. Design of representative prototype hydrodynamic boundary conditions including: (1) the definition of five storm cases A–E combined from local storm surge levels and sea level rise scenarios; (2) local mean wave conditions for two consecutive test series and (3) an exemplary time series from a storm surge event at the study area in 2013.

flume to record the dune face every 15 s through a lateral observation window. A solid-state laser scanner (*Blickfeld Cube 1*) was installed in front of the dune model to capture the subaerial dune face at a constant frame rate of 0.68 Hz. Due to its seaward position, the laser scanner only recorded the seaward subaerial dune face. Consequently, sediment deposition on the landward side of the dune caused by overtopping or breaching was outside the scanner's field of view and therefore not included in the analysis. A detailed description of key lidar features

Table 2
Experimental program for all tests performed.

Storm case	No. of tests	Test series	d (m)	$H_{s,measured}$ (m)	$T_{p,measured}$ (s)	t_{SSL} (min)	Flooding hazard regime	Erosion hazard regime
A	2	1	0.42	0.104–0.107	2.37–2.43	113	Collision	Dune face erosion
		2	0.42	0.160–0.161	2.51–2.64	113	Collision	Dune retreat
B	2	1	0.47	0.104–0.105	2.37–2.39	113	Collision	Dune face erosion
		2	0.47	0.155–0.156	2.58–2.73	113	Collision	Dune retreat
C	2	1	0.50	0.104–0.104	2.37–2.39	113	Collision	Dune retreat
		2	0.50	0.155–0.155	2.59–2.73	113	Collision	Dune retreat
D	2	1	0.54	0.103–0.104	2.37–2.43	113	Collision	Dune retreat
		2	0.54	0.153–0.153	2.50–2.61	113	Collision-Overwash	Dune retreat
E	1	1	0.59	0.101	2.39	113	Collision	Dune retreat
		2	0.59	0.150	2.61	45	Overwash-breaching	Dune retreat

and the applied measurement procedure are given by Mehrtens et al. (2025).

2.5. Data analysis

Water surface elevations measured at the wave gauges were used to analyze incoming wave statistics for each test. A 5-point moving average filter was applied to smooth the signal as well as a high-pass filter to cutoff low frequency ranges ($f_p < 0.1$ Hz). Significant wave height H_s was determined as $H_{1/3}$ using zero down-crossing procedure. Fast Fourier transform (FFT) technique was applied to determine the peak period T_p based on the peak wave frequency ($f_p = 1/T_p$). Since single wave gauges within the wave gauge array did not produce reliable measurements during multiple tests, no comparative wave reflection analyses have been carried out. The analysis of the solid-state laser scanner, including point-cloud filtering and data interpolation followed the methodology described by Mehrtens et al. (2025). Due to the test duration of 226 min and the constant sampling frequency of 0.68 Hz, the lidar scanned a total of 9220 frames with individual 3D point clouds. By applying a threshold filter for the relative intensity of each reflected laser pulse in a scan pattern, those frames were excluded, in which the subaerial dune face above SWL has not been captured reliable (e.g., due to wave runup and breaking waves). To minimize potential boundary effects from the flume sidewalls on the quantitative analysis, all data points within 20 cm from both sidewalls were excluded before each 3D point cloud was interpolated onto a regular yz-grid with constant increments of $\Delta y = \Delta z = 0.01$ m. Erosion volumes were calculated individually for each cross-shore profile line as the difference between the initial profile and the measured profile above still water level after a certain period of time, following the approach described by Van Gent et al. (2008). Therefore, the initial reference area above the still water level was determined individually for each storm case using the corresponding experimental SWL.

3. Results

3.1. Temporal dune profile development under rising storm surge level scenarios

Fig. 3 illustrates the temporal development of investigated dune profiles over two consecutive test series, comparing different storm cases A–E with scaled experimental water depths ranging from $d = 0.42$ m to $d = 0.59$ m. Unlike past contributions, this work presents novel high-resolution cross-shore profiles of erosive tendencies at very high temporal resolution in a continuous fashion during wave attack. Fig. 3 displays all extracted longitudinal cross-shore profiles along the flume center line at $y = 0.0$ m, with subaerial dune profile lines above the still water depth color-coded according to their corresponding experimental timestamps for test series 1 and 2. Due to the lidar analysis procedure, which only processes frames that reliably contain the entire dune face above SWL, the total number of extracted frames varies for test series 1 and 2 for all storm cases. With exception for test series 1 of storm case D, the number of extracted frames range from 4012 frames for test series 1 of storm case B to 665 frames for test series 2 of storm case E. The reduced number of 665 frames resulted from a shortened test duration of 45 min (see Table 2) due to dune breaching (see Fig. 4). Despite these variations, the overall high temporal resolution for all test runs enables detailed tracking of key dune erosion processes such as notching and subsequent slumping.

For all storm cases A–E, the dune profile development follows a periodic sequence of initial scarp formation, notching, dune face collapsing, and offshore-directed transport of slumped sediments. The frequency of notching and slumping phases increased with rising SWL, ranging from 9 distinct phases in storm case A to 14 in storm case E. The SWL plays a crucial role in the erosion process, as it defines the vertical zone of wave impact on the dune face and governs the prevailing flooding hazard regime. While the temporal sequence of notch formation patterns on the subaerial dune face remained consistent across all storm scenarios, the vertical elevation of notches varied systematically. In storm case A, the first prominent notch formed at a vertical elevation of $z = 0.54$ m, approximately 0.12 m above the corresponding SWL. As erosion progressed and the dune profile flattened over time, subsequent notches developed at incrementally higher elevations, with a final notch at $z = 0.60$ m for storm case A. The overall trend of rising notch elevation with increasing SWL was evident in all storm cases, with final notch elevations of $z = 0.67$ m in storm case C and $z = 0.70$ m in storm case E.

For lower storm cases A and B, with water depths of $d = 0.42$ m and $d = 0.47$ m, respectively, dune erosion during test series 1 remains confined to the seaward swash zone in front of the dune crest at $x = 8.2$ m, classifying both cases as '*dune face erosion*' according to the erosion hazard scale (see Table 2). By the end of test series 2, increased wave conditions led to further dune erosion in both cases, resulting in a transition to the '*dune retreat*' category of the erosion hazard scale. This progression was marked by landward retreat of the dune crest to $x = 8.33$ m and $x = 8.57$ m, respectively, indicating substantial profile retreat beyond the initial dune face position. For storm case C, the elevated water depth of $d = 0.5$ m led to dune erosion reaching the frontal dune crest section after test series 1, which intensified by the end of test series 2, causing an increased profile retreat to $x = 8.74$ m. Under the increased SWL in storm case D, with a water depth of $d = 0.54$ m, dune retreat progressed nearly to the landward limit of the dune crest at $x = 8.95$ m, by the end of test series 2. During test series 2, storm case D remained predominantly within the '*collision*' regime, while intermittent overtopping by a limited number of waves indicated the onset of a transition towards an '*overwash*' regime. However, no measurable landward sediment deposition was observed, indicating that sustained '*overwash*' conditions were not fully established during the experiment (see Table 2).

For storm case E, with a maximum water depth of $d = 0.59$ m, a large portion of the dune crest eroded up to $x = 8.77$ m under the prevailing '*collision*' regime during test series 1, indicating a substantial

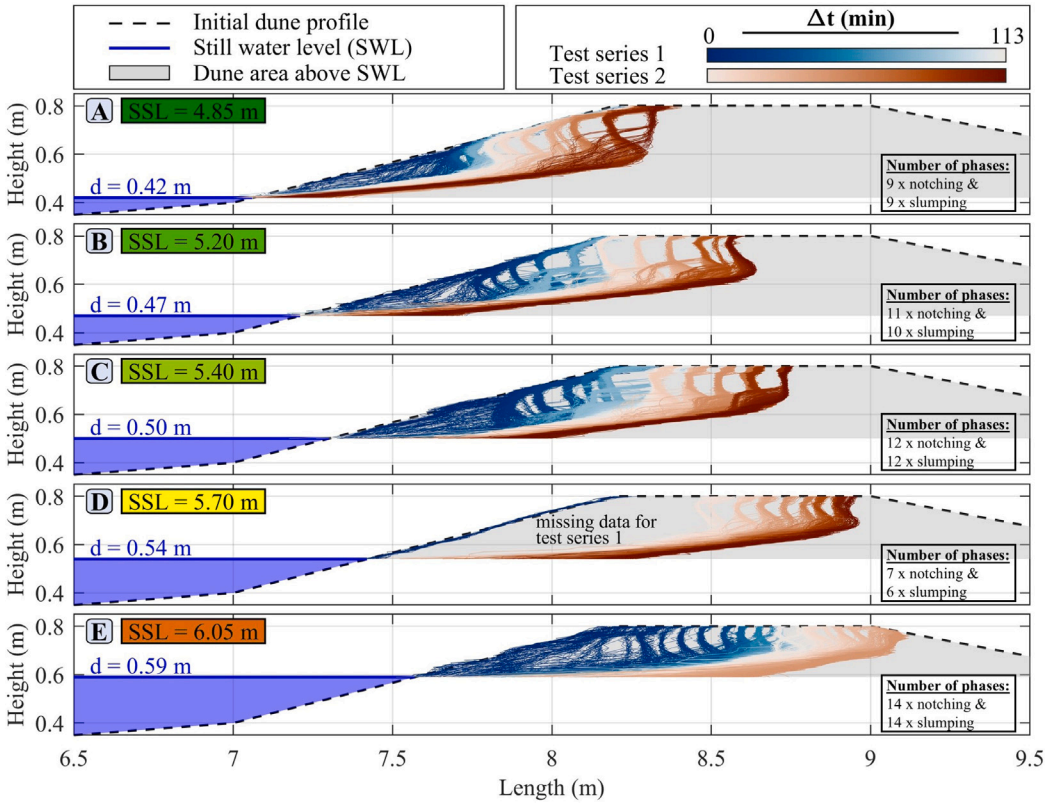


Fig. 3. Temporal dune profile development along the flume center line measured by the lidar and the number of notching and slumping phases for: storm case A with d = 0.42 m; storm case B with d = 0.47 m; storm case C with d = 0.50 m; storm case D with d = 0.54 m, and storm case E with d = 0.59 m. The color gradients illustrate the temporal evolution within each test series and the transition from the first to the second storm event.

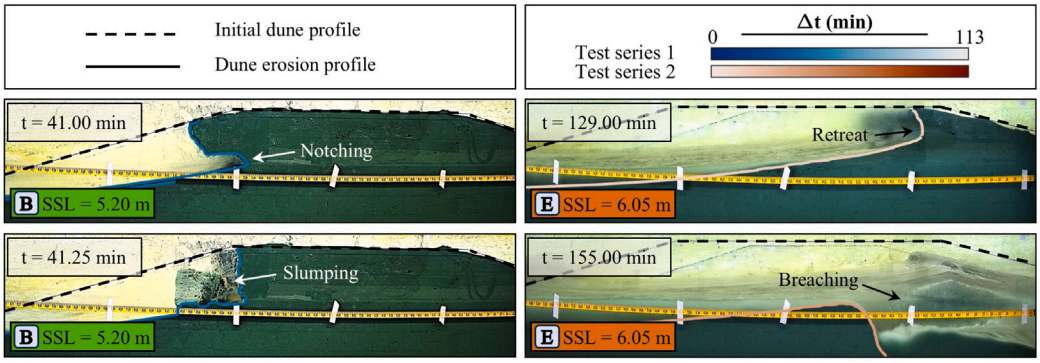


Fig. 4. Side-looking view at the observation window of characteristic notching and slumping under storm case B with d = 0.47 m (left); characteristic dune face retreat and breaching under storm case E with d = 0.59 m (right). The images are to be intended as a qualitative visualization of the erosion processes adjacent to the flume sidewall.

'*dune retreat*' hazard scale. During test series 2, increased wave conditions caused a transition from '*collision*' to '*overwash*' regime, with frequent wave overtopping initiating further dune retreat up to the landward edge of the crest. This progression ultimately resulted in a major dune breach, with intensified water flow, eroding and transporting large portions of the remaining dune profile to the landward side (see Fig. 4). Since dune breaching represented the final failure state of the protection system, the experiment was intentionally terminated after a total duration of 158 min. Consequently, storm case E remains directly comparable with the other storm cases during the observation period prior to breaching. However, due to the shortened duration of the second test series, the final post-storm erosion volume cannot be quantitatively compared with storm cases A–D.

3.2. Temporal erosion volume development under rising storm surge level scenarios

Fig. 5 provides an overview of the temporal erosion volume development for all tests with the top section displaying mean erosion volumes above SWL across the dune width for all extracted frames. Polynomial curve fitting was applied to each test run, encompassing both test series 1 and 2, to compensate for single outliers caused by erosion-related processes, such as slumped sediment chunks accumulating in front of newly formed scarps, which obscure the underlying dune profile and lead to underestimations of erosion volume (as described by Mehrtens et al. (2025)). By comparing the initial and repetition tests for storm case A – D, a consistently high temporal agreement was observed between individual test runs, with polynomial curves exhibiting

correlation coefficients of at least R = 0.99. As no data was available for test series 1 of storm case D, erosion volumes are not displayed for either test. For the remaining four storm cases, highest erosion rates occurred consistently within the first 5 min of test series 1, ranging from 0.008 to 0.018 $\frac{m^3}{m*min}$ for cases A to E, indicating substantial dune profile changes during the initial test phase. Towards the end of test series 1, erosion rates gradually stagnated across all storm cases as equilibrium profiles with more gently sloped dune faces developed. In equilibrium profiles, a greater proportion of incoming waves break prior to reaching the dune face, stipulated by lower water levels, as dune sediments are deposited close to the SWL elevation and below. By the start of test series 2, erosion volumes increased again as a result of intensified, more energetic wave conditions that eroded rear areas of the dune crest, with reduced peak erosion rates across all storm cases in the range of 0.002 to 0.003 $\frac{m^3}{m*min}$ followed by a gradual decline in erosion rate due to the repeated formation of newly developing equilibrium profiles. Corresponding to the dune profile developments in Fig. 3, temporal erosion volumes steadily increase with rising SWLs from storm cases A–E at comparable timestamps. As dune breaching occurred in storm case E after 155 min, the erosion volume above the respective SWL of d = 0.59 m increased to 0.22 m^3/m. In comparison, storm cases B–D resulted in even higher erosion volumes, reaching up to 0.26 m^3/m at the end of test series 2, without any dune breaching. These variations result from wave run-up occurring at elevated levels for increased water depths, causing erosion in the upper dune crest, where sediment availability is more limited compared to the lower dune core. To facilitate a targeted comparison of different storm cases, the bottom section of Fig. 5 illustrates mean percentages of eroded dune area above the respective SWLs, ranging from d = 0.42 to d = 0.59 m for each scenario. In storm cases A–C, less than 25% of the dune area above the respective SWLs was eroded at the end of test series 1, whereas for the highest storm case E, 50% of the available sediment area had already been lost. Subsequently, during test series 2, the percentage of eroded dune mass increased up to approximately 70% for storm case E, ultimately leading to partial dune breaching on one side. In contrast, storm cases A–D illustrate that by the end of test series 2, a sufficiently large portion of dune area above the respective SWLs remains uneroded, preventing dune breaching. Similar findings are additionally presented in Fig. 6, where the erosion volume above SWL and percentage of eroded dune area above SWL are plotted against the tested SWLs.

4. Discussion

This study presents novel insights into the erosion behavior of a bare coastal dune model subjected to progressively rising still water levels (SWLs), representing prototype storm surge level (SSL) scenarios associated with projected sea-level rise along the German North Sea coast, derived from Gaslikova et al. (2013). While previous laboratory studies have extensively investigated characteristic dune erosion mechanisms, including scarping, notching, slumping, collision, and overwash processes under different hydrodynamic conditions (Van Gent et al., 2008; D'Alessandro and Tomasicchio, 2016; Bond et al., 2023; Conti et al., 2024), the present study complements these investigations by systematically isolating the influence of increasing still water level on dune erosion using a geometrically representative prototype profile and identical experimental procedures across several storm cases. By systematically varying the experimental SWL in the 1:7 scaled physical experiments, this research contributes detailed spatio-temporal data on characteristic erosion processes and the residual protection level. The comparison of the captured lidar data in Fig. 3 with the side-view observations at the flume wall in Fig. 4 indicate slight transverse variations in the position and timing of dune erosion. This observation supports the applied data processing approach, in which all lidar data within 20 cm of both sidewalls were excluded from the interpolation to minimize their influence on the quantitative assessment. At the same time, the side-view images provide valuable complementary information by enabling a direct visual observation of the characteristic temporal sequence of notching, scarp formation and subsequent slumping.

The experimental results reveal a non-linear trend of increasing dune erosion severity with rising SSLs (see Fig. 6). At lower water levels during a first storm surge event (storm case A and B, representing current storm surge levels without projected SLR), dune erosion remained largely confined to the dune face, with limited crest retreat and no signs of breaching. As the SSL increased in storm cases C to E, the experiments documented significant retreat of the dune crest and a transition from collision to overwash regime. During a subsequent storm event for storm case E (representing a projected SLR of 1.2 m by 2100 based on RCP8.2), repeated wave overtopping led to crest lowering, partial breaching and landward directed sediment transport. While the fundamental sequence of scarping, notching, slumping, and sediment removal remains consistent with previous studies (Erikson et al., 2007; Bond et al., 2023; Van Wiechen et al., 2024), rising SSLs induce a vertical shift of these processes into the upper dune section. This upward displacement corresponds with an increased frequency of slumping events, consistent with observations by Conti et al. (2024), and subsequently heightens the vulnerability to dune failure due to the diminished volume of protective sand at the dune crest.

Beyond the observed process transitions, the present study demonstrates that the proportion of eroded dune area above the still water level provides complementary information to the conventional erosion volume. While erosion volume quantifies the total amount of sediment removed, it does not necessarily reflect how much of the protective dune area remains available to resist overtopping and breaching. This becomes particularly evident for storm cases D and E, where similar erosion volumes are associated with substantially different residual protection levels due to the upward migration of erosion towards the dune crest. Expressing erosion relative to the initial dune area above the respective still water level therefore provides a physically meaningful measure of the remaining protective capacity of the dune. Consequently, future assessments of dune stability in the context of storm surge and sea-level rise scenarios should incorporate both absolute erosion volumes and relative geometric indicators, such as the percentage of remaining dune profile above SWL, to more accurately capture changes in protective capacity and inform adaptive coastal management strategies.

Despite the consistent modeling of the beach-dune profile in alignment with local hydrodynamic conditions, several limitations of the experimental model setup are to be acknowledged. The selected geometries and hydrodynamics provide realistic experimental conditions for investigating specific dune erosion processes, but unavoidable simplifications such as the omission of vegetation (similar to D'Alessandro and Tomasicchio, 2016; Bond et al., 2023; Conti et al., 2024) and adjacent coastal features limit a direct quantitative transfer of erosion volumes or breaching thresholds to the prototype scale. Consequently, the principal contribution of the present study lies in identifying relative changes in erosion mechanisms, hazard-regime transitions, and residual dune protective capacity under progressively increasing still water levels rather than predicting an exact protection level of the investigated dune system.

The geometric model representation focused solely on the established dune ridge, omitting any additional elements, such as foredunes, buffering salt marshes, and adjacent dune forest belts. As demonstrated by previous studies, natural landscapes such as a salt marsh (Zhang et al., 2020; Keimer et al., 2024), and an incipient foredune (Mehrtens et al., 2023; Sánchez-Artús et al., 2024) can play important roles in dissipating wave energy erosion buffering, thereby enhancing the overall resilience of the coastal barrier system. Additionally, the experimental setup did not incorporate native dune vegetation, which is a key ecological component influencing dune stability (Maximiliano-Cordova et al., 2019; Gao et al., 2020). Numerous experimental studies

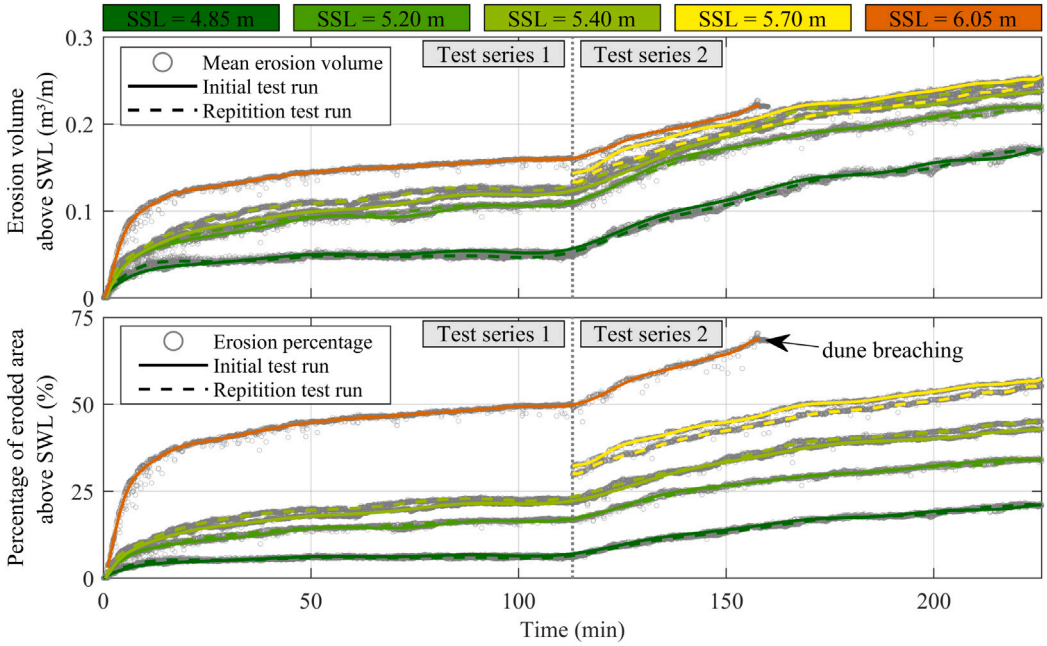


Fig. 5. Temporal development of (top) mean erosion volumes above SWL and (bottom) mean percentages of eroded dune area above SWL under storm cases A–E. Gray circles represent individual data points; solid and dashed lines indicate polynomial curve fits.

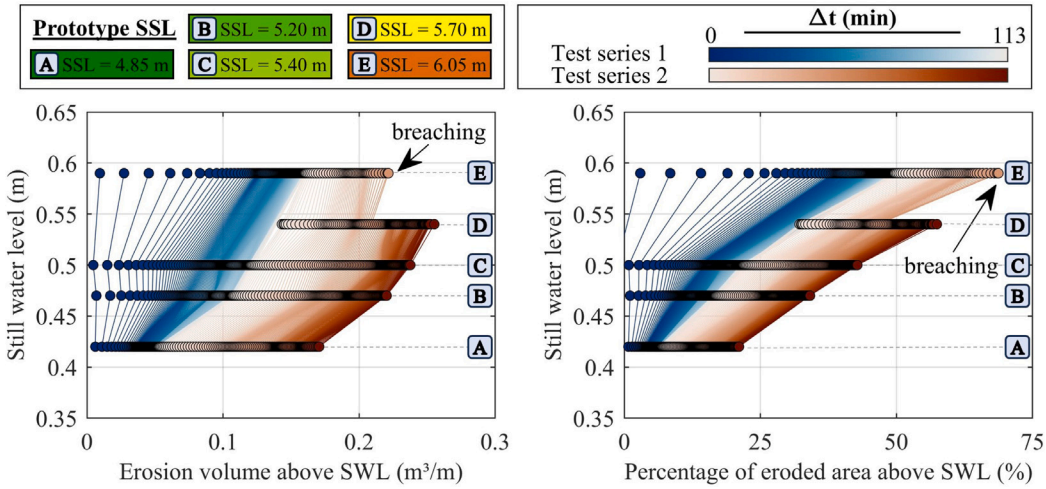


Fig. 6. Influence of different still water levels versus: temporal erosion volumes above SWL (left) and percentages of eroded dune area above SWL (right).

have demonstrated that vegetation can either reinforce dune stability against erosion by enhancing sediment cohesion (Bryant et al., 2019; Figlus et al., 2022) or, under certain conditions, accelerate dune erosion dynamics by increased water penetration into the sediment (Feagin et al., 2023).

Furthermore, this research was conducted with the working hypothesis that the present dune profile remains invariant in the face of gradual SLR to facilitate systematic modeling and render results comparable. However, expected long-term changes in beach width, nearshore bathymetry, foredune development, and vegetation cover are likely to alter wave transformation and dune erosion behavior. Consequently, reproducing the present-day coastal profile with all existing landscape features does not necessarily provide a realistic representation of future climate conditions. Nevertheless, the absence of such landscape components results in a conservative estimation of the overall dune system protection level, leaving several future research needs such as: (i) the incorporation of established dune vegetation, (ii) the buffering capacity of a growing foredune system against erosion (Mehrtens et al., 2024; Schweiger et al., 2025), (iii) the effect of an established coniferous dune forest on dune resilience (Lojek et al., 2025), and (iv) the impact of oblique wave attack and resulting longitudinal sediment transport processes on dune erosion.

CRediT authorship contribution statement

Björn Mehrtens: Writing – original draft, Visualization, Methodology, Investigation, Formal analysis, Data curation, Conceptualization. **Oliver Lojek:** Writing – review & editing, Supervision, Resources, Project administration, Methodology, Conceptualization. **Lukas Ahrenbeck:** Writing – review & editing, Investigation, Formal analysis, Data curation. **Viktoria Kosmalla:** Writing – review & editing, Investigation, Formal analysis, Data curation. **Thea Bölker:** Writing – review & editing, Investigation, Data curation. **David Schürenkamp:** Writing – review & editing, Validation, Resources, Project administration, Funding acquisition, Conceptualization. **Nils Goseberg:** Writing – review & editing, Validation, Supervision, Resources, Project administration, Funding acquisition, Conceptualization.

Declaration of competing interest

The authors declare that they have no known competing financial interests or personal relationships that could have appeared to influence the work reported in this paper.

Acknowledgments

This work is part of the research project "Sandküste St. Peter-Ording" (FKZ 3520685C16) funded by the German Federal Agency for Nature Conservation (BfN), the German Federal Ministry for the Environment, Nature Conservation, Nuclear Safety and Consumer Protection (BMUV) and the Ministry for Energy Transition, Climate Protection, Environment and Nature (MELUR). Thanks to the Agency for Coastal Protection, National Parks, and Ocean Protection Schleswig-Holstein (LKN.SH) for providing digital terrain data from the study area as well as the German Federal Institute of Hydrology (BfG) for providing water level data from local gauging stations.

Data availability

Data will be made available on request.

References

Barbier, E., Hacker, S., Kennedy, C., Koch, E., Stier, A., Silliman, B., 2011. The value of estuarine and coastal ecosystem services. Ecol. Monograph. 81, 169–193. http://dx.doi.org/10.1890/10-1510.1.

Berard, N.A., Mulligan, R.P., Da Silva, A.M.F., Dibajnia, M., 2017. Evaluation of xbeach performance for the erosion of a laboratory sand dune. Coast. Eng. 125, 70–80. http://dx.doi.org/10.1016/j.coastaleng.2017.04.002.

Bond, H., Wengrove, M., Puleo, J., Pontiki, M., Evans, T.M., Feagin, R.A., 2023. Beach and dune subsurface hydrodynamics and their influence on the formation of dune scarps. J. Geophys. Res. Earth Surf 128, e2023JF007298. http://dx.doi.org/10.1029/2023JF007298.

Bryant, D.B., Anderson Bryant, M., Sharp, J.A., Bell, G.L., Moore, C., 2019. The response of vegetated dunes to wave attack. Coast. Eng. 152, 103506. http://dx.doi.org/10.1016/j.coastaleng.2019.103506.

Calafat, F.M., Wahl, T., Tadesse, M.G., Sparrow, S.N., 2022. Trends in europe storm surge extremes match the rate of sea-level rise. Nature 603, 841–845. http://dx.doi.org/10.1038/s41586-022-04426-5.

Conti, S., Splinter, K.D., Booth, E., Djadjiguna, D., Turner, I.L., 2024. Observations on the role of internal sand moisture dynamics in wave-driven dune face erosion. Geomorphology 462, 109331. http://dx.doi.org/10.1016/j.geomorph.2024.109331.

D'Alessandro, F., Tomasicchio, G.R., 2016. Wave–dune interaction and beach resilience in large-scale physical model tests. Coast. Eng. 116, 15–25. http://dx.doi.org/10.1016/j.coastaleng.2016.06.002.

D'Alessandro, F., Tomasicchio, G.R., Frega, F., Leone, E., Francone, A., Pantusa, D., et al., 2022. Beach–Dune system morphodynamics. JMSE 10, 627. http://dx.doi.org/10.3390/jmse10050627.

De Jong, B., Keijsers, J., Riksen, M., Krol, J., Slim, P., 2014. Soft engineering vs. a dynamic approach in coastal dune management: A case study on the north sea barrier island of Ameland, The Netherlands. J. Coast. Res. 30, 670. http://dx.doi.org/10.2112/JCOASTRES-D-13-00125.1.

Dionísio António, S., van der Werf, J., Horstman, E., Cáceres, I., Alsina, J., van der Zanden, J., Hulscher, S., 2023. Influence of beach slope on morphological changes and sediment transport under irregular waves. JMSE 11, 2244. http://dx.doi.org/10.3390/jmse11122244.

Dissanayake, P., Brown, J., Wisse, P., Karunarathna, H., 2015. Comparison of storm cluster vs isolated event impacts on beach/dune morphodynamics. Estuar. Coast. Shelf Sci. 164, 301–312. http://dx.doi.org/10.1016/j.ecss.2015.07.040.

Erikson, L.H., Larson, M., Hanson, H., 2007. Laboratory investigation of beach scarp and dune recession due to notching and subsequent failure. Mar. Geol. 245, 1–19. http://dx.doi.org/10.1016/j.margeo.2007.04.006.

Feagin, R.A., Innocenti, R.A., Bond, H., Wengrove, M., Huff, T.P., Lomonaco, P., et al., 2023. Does vegetation accelerate coastal dune erosion during extreme events? Sci. Adv. 9, eadg7135. http://dx.doi.org/10.1126/sciadv.adg7135.

Figlus, J., Kobayashi, N., Gralher, C., Iranzo, V., 2011. Wave overtopping and overwash of dunes. J. Waterw. Port, Coast. Ocean. Eng. 137, 26–33. http://dx.doi.org/10.1061/(ASCE)WW.1943-5460.0000060.

Figlus, J., Sigren, J.M., Feagin, R.A., Armitage, A.R., 2022. The unique ability of fine roots to reduce Vegetated Coastal dune erosion during wave collision. Front. Built Env. 8, 904837. http://dx.doi.org/10.3389/fbuil.2022.904837.

Gao, J., Kennedy, D.M., Konlechner, T.M., 2020. Coastal dune mobility over the past century: A global review. Prog. Phys. Geogr.: Earth Environ. 44, 814–836. http://dx.doi.org/10.1177/0309133320919612.

Gaslikova, L., Grabemann, I., Groll, N., 2013. Changes in North sea storm surge conditions for four transient future climate realizations. Nat. Hazards 66, 1501–1518. http://dx.doi.org/10.1007/s11069-012-0279-1.

Ghasemi, P., Montoya, B.M., Evans, T.M., Wengrove, M.E., 2024. Geotechnical properties and performance of large-Scale Coastal dunes reinforced by biocementation under hurricane wave conditions. J. Geotech. Geoenviron. Eng. 150, 04024103. http://dx.doi.org/10.1061/JGGEFK.GTENG-12483.

Gracia, A., Rangel-Buitrago, N., Oakley, J.A., Williams, A.T., 2018. Use of ecosystems in coastal erosion management. Ocean & Coastal Management 156, 277–289. http://dx.doi.org/10.1016/j.ocecoaman.2017.07.009.

Hagen, R., Plüß, A., Schrage, N., Dreier, N., 2020. EasyGSH-DB: Themengebiet - synoptische hydrodynamik. http://dx.doi.org/10.48437/02.2020.K2.7000.0004.

Hanley, M.E., Hoggart, S., Simmonds, D.J., Bichot, A., Colangelo, M.A., Bozzeda, F., et al., 2014. Shifting sands? Coastal protection by sand banks, beaches and dunes. Coast. Eng. 87, 136–146. http://dx.doi.org/10.1016/j.coastaleng.2013.10.020.

Harley, M.D., Masselink, G., Ruiz de Alegría-Arzaburu, A., Valiente, N.G., Scott, T., 2022. Single extreme storm sequence can offset decades of shoreline retreat projected to result from sea-level rise. Commun Earth Environ. 3, http://dx.doi.org/10.1038/s43247-022-00437-2.

Hesp, P., 2002. Foredunes and blowouts: Initiation, geomorphology and dynamics. Geomorphology 48, 245–268. http://dx.doi.org/10.1016/S0169-555X(02)00184-8.

Huynh, L.T.M., Su, J., Wang, Q., Stringer, L.C., Switzer, A.D., Gasparatos, A., 2024. Meta-analysis indicates better climate adaptation and mitigation performance of hybrid engineering-natural coastal defence measures. Nat. Commun. 15, 2870. http://dx.doi.org/10.1038/s41467-024-46970-w.

Irish, J.L., Cheng, W., Weiss, R., Patch, S.M., Beever, M.A., 2024. Influence of belowground biomass on barrier-island evolution during storms: A computational parameter study. J. Waterw. Port, Coast. Ocean. Eng. 150, 04024003. http://dx.doi.org/10.1061/JWPED5.WWENG-2047.

Jänicke, L., Ebener, A., Dangendorf, S., Arns, A., Schindelegger, M., Niehüser, S., et al., 2021. Assessment of tidal range changes in the north sea from 1958 to 2014. J. Geophys. Res. Ocean. 126, e2020JC016456. http://dx.doi.org/10.1029/2020JC016456.

Keimer, K., Kind, F., Prüter, I., Kosmalla, V., Lojek, O., Schürenkamp, D., et al., 2024. From seasonal field study to surrogate modeling: Investigating the biomechanical dynamics of elymus sp. in salt marshes. Limnol. Ocean. Methods 22, 416–436. http://dx.doi.org/10.1002/lom3.10616.

Lansu, E.M., Reijers, V.C., Höfer, S., Luijendijk, A., Rietkerk, M., Wassen, M.J., et al., 2024. A global analysis of how human infrastructure squeezes sandy coasts. Nat. Commun. 15, 432. http://dx.doi.org/10.1038/s41467-023-44659-0.

Leaman, C.K., Harley, M.D., Splinter, K.D., Thran, M.C., Kinsela, M.A., Turner, I.L., 2021. A storm hazard matrix combining coastal flooding and beach erosion. Coast. Eng. 170, 104001. http://dx.doi.org/10.1016/j.coastaleng.2021.104001.

Lee, E., van Dang, H., Shin, S., Yoo, J., Park, H., 2024. Observations of wave run-up affected by dune scarp during storm conditions: a two dimensional large-scaled movable bed experiment. Front. Mar. Sci. 11, 1369418. http://dx.doi.org/10.3389/fmars.2024.1369418.

Liang, B., Qu, Z., Lee, D.Y., Zhang, X., 2023. Laboratory investigation of hydrodynamic and sand dune morphology changes under wave overwash. J. Geophys. Res. Ocean. 128, e2023JC019845. http://dx.doi.org/10.1029/2023JC019845.

Lojek, O., Mehrtens, B., Kosmalla, V., Ahrenbeck, L., Schweiger, C., Schürenkamp, D., Goseberg, N., 2025. Modeled influence of large-scale tree cover on the erosion process of coastal dunes. Int. Conf. Coast. Eng. 38, 40. http://dx.doi.org/10.9753/icce.v38.sediment.4.

Ma, M., Huang, W., Jung, S., Oslon, C., Yin, K., Xu, S., 2024. Evaluating vegetation effects on wave attenuation and dune erosion during hurricane. JMSE 12, 1326. http://dx.doi.org/10.3390/jmse12081326.

Maximiliano-Cordova, C., Martínez, M.L., Silva, R., Hesp, P.A., Guevara, R., Landgrave, R., 2021. Assessing the impact of a winter storm on the beach and dune systems and erosion mitigation by plants. Front. Mar. Sci. 8, http://dx.doi.org/10.3389/fmars.2021.734036.

Maximiliano-Cordova, C., Salgado, K., Martinez, M.L., Mendoza, E., Silva, R., Guevara, R., Feagin, R.A., 2019. Does the functional richness of plants reduce wave erosion on Embryo Coastal dunes? Estuar. Coasts 42, 1730–1741. http://dx.doi.org/10.1007/s12237-019-00537-x.

Maximiliano-Cordova, C., Silva, R., Mendoza, E., Chávez, V., Martínez, M.L., Feagin, R.A., 2023. Morphological performance of vegetated and non-Vegetated Coastal dunes with rocky and geotextile tube cores under storm conditions. JMSE 11, 2061. http://dx.doi.org/10.3390/jmse11112061.

Mehrtens, B., Lojek, O., Bölker, T., Ahrenbeck, L., Kosmalla, V., Schweiger, C., et al., 2024. Experimental investigation Of Coastal foredune erosion. http://dx.doi.org/10.59490/coastlab.2024.794, CoastLab 2024: Physical Modelling in Coastal Engineering and Science.

Mehrtens, B., Lojek, O., Kosmalla, V., Bölker, T., Goseberg, N., 2023. Foredune growth and storm surge protection potential at the eiderstedt peninsula, Germany. Front. Mar. Sci. 9, 1020351. http://dx.doi.org/10.3389/fmars.2022.1020351.

Mehrtens, B., Vinkelau, L., Bölker, T., Lojek, O., Ahrenbeck, L., Schweiger, C., et al., 2025. Benchmarking overview on methods for spatiotemporal detection of dune erosion in physical modeling. J. Waterw. Port, Coast. Ocean. Eng. 151, 04025012. http://dx.doi.org/10.1061/JWPED5.WWENG-2138.

Nehren, U., Thai, H.H.D., Marfai, M.A., Raedig, C., Alfonso, S., Sartohadi, J., Castro, C., 2016. Ecosystem services of coastal dune systems for hazard mitigation: Case studies from Vietnam, Indonesia, and Chile. In: Renaud, F.G., Sudmeier-Rieux, K., Estrella, M., Nehren, U. (Eds.), Ecosystem-Based Disaster Risk Reduction and Adaptation in Practice. Springer International Publishing, Cham, pp. 401–433. http://dx.doi.org/10.1007/978-3-319-43633-3_18.

Odériz, I., Knöchelmann, N., Silva, R., Feagin, R.A., Martínez, M.L., Mendoza, E., 2020. Reinforcement of vegetated and unvegetated dunes by a rocky core: A viable alternative for dissipating waves and providing protection? Coast. Eng. 158, 103675. http://dx.doi.org/10.1016/j.coastaleng.2020.103675.

Palmsten, M.L., Holman, R.A., 2012. Laboratory investigation of dune erosion using stereo video. Coast. Eng. 60, 123–135. http://dx.doi.org/10.1016/j.coastaleng.2011.09.003.

Sallenger, A.H., 2000. Storm impact scale for barrier islands. J. Coast. Res. 16, 890–895.

Sánchez-Artús, X., Subbiah, B., Gracia, V., Espino, M., Grifoll, M., Espanya, A., Sánchez-Arcilla, A., 2024. Evaluating barrier beach protection with numerical modelling. A practical case. Coast. Eng. 191, 104522. http://dx.doi.org/10.1016/j.coastaleng.2024.104522.

Schweiger, C., Mehrtens, B., Bölker, T., Lojek, O., Ahrenbeck, L., Schürenkamp, D., Goseberg, N., 2025. Numerical study on the influence of coastal foredunes on storm-induced erosion. Int. Conf. Coast. Eng. 38, 35. http://dx.doi.org/10.9753/icce.v38.sediment.35.

Sedrati, M., Dalour, L., Bulot, G., Metge, N., 2025. Nature-based solutions for coastal dune restoration: The case study of AlgoBox in South Brittany, France. Ecol. Eng. 210, 107440. http://dx.doi.org/10.1016/j.ecoleng.2024.107440.

Sievers, J., Malte, R., Milbradt, P., 2020. EasyGSH-DB: Bathymetrie (1996–2016). http://dx.doi.org/10.48437/02.2020.K2.7000.0002, URL https://datenrepository.baw.de/trefferanzeige?cmd=doShowDocument&docuuid=8a917a5c-aa8c-4a74-a10e-12cfa0c41f8b&plugid=/ingrid-group:iplug-ige-datenrepo.

Silva, R., Martínez, M.L., Odériz, I., Mendoza, E., Feagin, R.A., 2016. Response of vegetated dune–beach systems to storm conditions. Coast. Eng. 109, 53–62. http://dx.doi.org/10.1016/j.coastaleng.2015.12.007.

Soulsby, R., 1997. Dynamics of Marine Sands: A Manual for Practical Applications. Emerald Publishing Limited, London.

Toledo, I., Pagán, J.I., López, I., Bañón, L., Aragonés, L., 2024. Analysis of the factors affecting erosion in the beach-dune system of Guardamar del Segura, Spain. CATENA 243, 108212. http://dx.doi.org/10.1016/j.catena.2024.108212.

Van Gent, M., van Thiel de Vries, J., Coeveld, E.M., Vroeg, J.H.d., van de Graaff, J., 2008. Large-scale dune erosion tests to study the influence of wave periods. Coast. Eng. 55, 1041–1051. http://dx.doi.org/10.1016/j.coastaleng.2008.04.003.

Van Wiechen, P.P.J., Mieras, R., Tissier, M.F.S., de Vries, S., 2024. Coastal dune erosion and slumping processes in the swash-dune collision regime based on field measurements. J. Geophys. Res. Earth Surf. 129, e2024JF007711. http://dx.doi.org/10.1029/2024JF007711.

Vousdoukas, M.J., Mentaschi, L., Hinkel, J., Ward, P.J., Mongelli, I., Ciscar, J.C., Feyen, L., 2020. Economic motivation for raising coastal flood defenses in Europe. Nat. Commun. 11, 2119. http://dx.doi.org/10.1038/s41467-020-15665-3.

Zarnetske, P.L., Ruggiero, P., Seabloom, E.W., Hacker, S.D., 2015. Coastal foredune evolution: The relative influence of vegetation and sand supply in the US Pacific northwest. J. R. Soc. Interface 12, http://dx.doi.org/10.1098/rsif.2015.0017.

Zhang, X., Lin, P., Gong, Z., Li, B., Chen, X., 2020. Wave attenuation by spartina alterniflora under macro-tidal and storm surge conditions. Wetlands 40, 2151–2162. http://dx.doi.org/10.1007/s13157-020-01346-w.